Journal of Materials Chemistry

www.rsc.org/materials

Volume 22 | Number 28 | 28 July 2012 | Pages 13857–14290

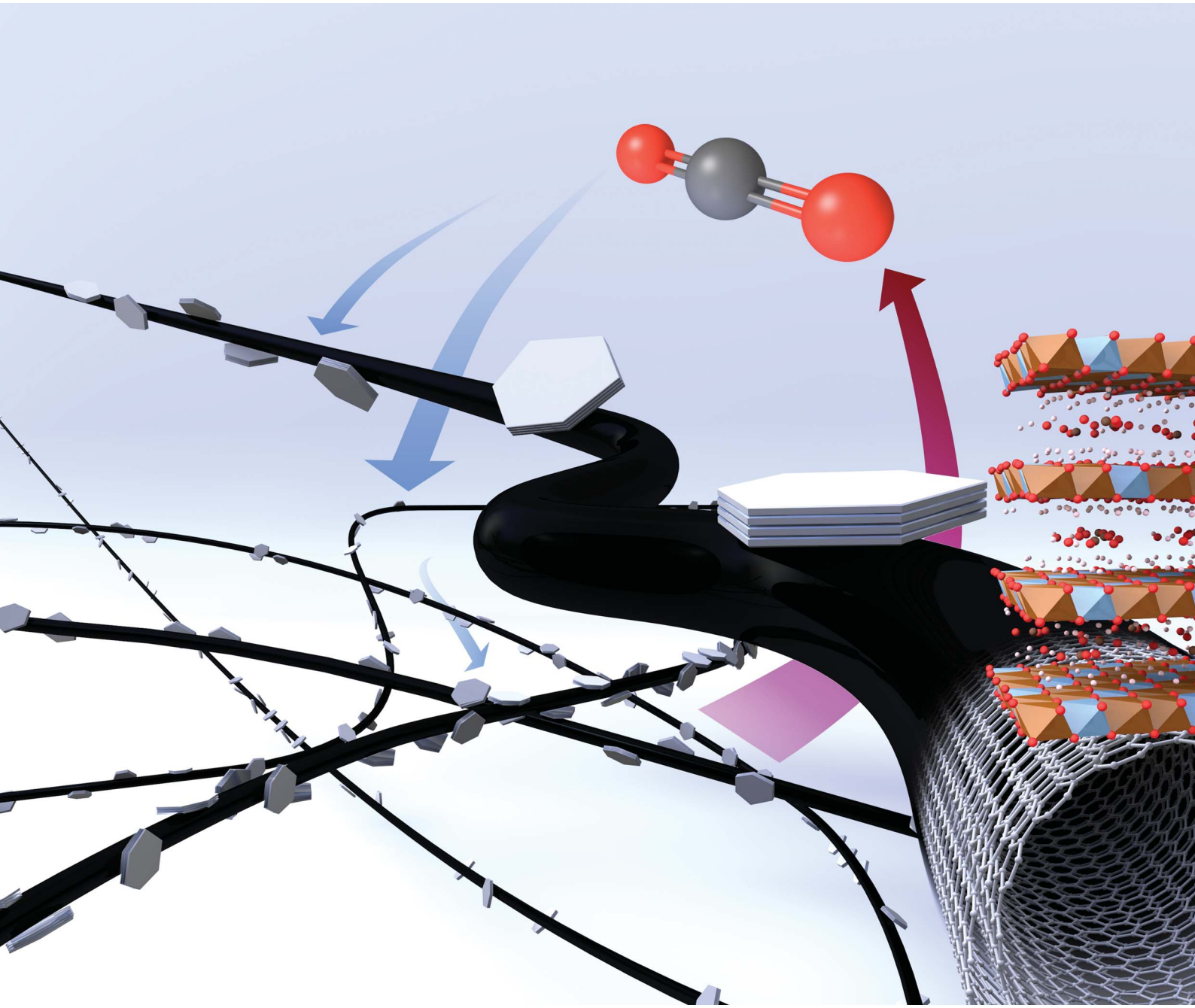

ISSN 0959-9428

RSC Publishing

PAPER

Ainara Garcia-Gallastegui *et al.*

Layered double hydroxides supported on multi-walled carbon nanotubes: preparation and CO_2 adsorption characteristics

0959-9428(2012)22:28;1-B

Journal of Materials Chemistry

Dynamic Article Links

Cite this: J. Mater. Chem., 2012, 22, 13932

www.rsc.org/materials

PAPER

Layered double hydroxides supported on multi-walled carbon nanotubes: preparation and CO_2 adsorption characteristics†

Ainara Garcia-Gallastegui,*[ab] Diana Iruretagoyena,[d] Mohamed Mokhtar,[c] Abdullah M. Asiri,[c] Sulaiman N. Basahel,[c] Shaeel A. Al-Thabaiti,[c] Abdulrahman O. Alyoubi,[c] David Chadwick[d] and Milo S. P. Shaffer*[a]

Received 4th January 2012, Accepted 20th April 2012
DOI: 10.1039/c2jm00059h

Layered double hydroxides (LDHs) are promising materials for CO_2 sorption, although improvements in performance are required for practical applications. In the current study, the CO_2 sorption capacity and multi-cycle stability were both increased by introducing an open supporting framework of multi-walled carbon nanotubes (MWNTs). This nanostructured inert network provides a high surface area, maximizing the gas accessibility and minimizing coarsening effects. Specifically, LDH nanoparticles were precipitated directly onto MWNTs, initially oxidised to ensure a favourable electrostatic interaction and hence a good dispersion. The dependence of the structural and physical properties of the Mg–Al LDH grown on MWNT supports has been studied, using electron microscopy, X-ray diffraction, thermogravimetric analysis (TGA), and BET surface area, and correlated with the CO_2 sorption capacity, established *via* TGA and temperature programmed desorption measurements. The use of a MWNT support was found to improve the absolute capacity and cycle stability of the hybrid adsorbent under dry conditions.

Introduction

Layered double hydroxides (LDHs), also known as hydrotalcite-like compounds, belong to a large class of synthetic two-dimensional (2D) nanostructured materials. Their structure is composed of positively charged $Mg(OH)_2$ layers in which divalent cations, octahedrally coordinated by hydroxyls, are partially substituted by trivalent cations resulting in positively charged layers with charge-balancing anions between them. The charge-neutral LDH structure can be represented by the general formula $(M^{2+}_{1-x}M^{3+}_{x}(OH)_2)^{x+}(A^{m-}_{x/m}\cdot nH_2O)^{x-}$ where M^{2+}, M^{3+} and A^{m-} commonly represent Mg^{2+}, Al^{3+} and CO_3^{2-} respectively. The wide variety of physicochemical properties that can be obtained by altering the nature of the metal cations, their molar ratios or the type of interlayer anions has attracted increasing attention from material chemists. Hydrotalcite-like compounds have found practical applications in areas such as catalysis, supercapacitors, pharmaceutics, photochemistry, electrochemistry and in sorption processes.[1,2]

Concerns about the increasing concentration of greenhouse gases in the atmosphere have stimulated the study of CO_2 capture and storage (CCS) processes including the use of solid sorbents.[3,4] LDHs are regarded as promising adsorbents for CO_2, for CCS and many other applications, showing high selectivity in the temperature range from 473 K to 723 K. Compared to other potential CO_2 solid adsorbents, such as calcium oxides, LDHs require less energy in regeneration and show superior multicycle stability.[3] In addition, they show fast adsorption-desorption kinetics and good performance in the presence of water, making them very attractive not only for pre-combustion CO_2 capture but also for applications involving CO_2 equilibria such as sorption-enhanced hydrogen production.[5–8] However, despite these positive adsorption properties, LDHs exhibit relatively low CO_2 adsorption capacities which limit their commercial use. In order to alleviate this weakness and to improve overall adsorption performance, several studies have focused on altering the chemistry of LDHs by exchanging their structural cations and anions and/or by incorporating alkali dopants such as potassium and caesium.[9–12] A parallel approach has been to support or combine LDHs with high surface area materials such as alumina,[13] zeolites[14] and carbons,[15] to increase the particle dispersion. When supported on a large fraction of carbon

[a]*Department of Chemistry, Imperial College London, South Kensington Campus, London SW7 2AZ, UK. E-mail: m.shaffer@imperial.ac.uk; Fax: +44(0)207 594 5801; Tel: +44(0)207 594 5825*
[b]*Bio Nano Consulting, 338 Euston Road, London NW1 3BT, UK. E-mail: ainara.garcia@bio-nano-consulting.com; Fax: +44(0)207 396 1056; Tel: +44(0)207 396 1050*
[c]*Department of Chemistry, Faculty of Science, King Abdulaziz University, Jeddah 21589, Saudi Arabia*
[d]*Department of Chemical Engineering, Imperial College London, South Kensington Campus, London SW7 2AZ, UK*

† Electronic supplementary information (ESI) available: Representative TEM image corresponding to the LDH/MWNT sample containing 62 wt% LDH where the LDH platelet thickness can be measured and adsorption-desorption nitrogen isotherms of LDH, oxidised MWNT and LDH/MWNT samples. See DOI: 10.1039/c2jm00059h

nanofibers (CNFs), Meis *et al.*[15] found that the apparent adsorption capacity per mass of activated Mg–Al LDHs increased by an order of magnitude, at 523 K, in the presence of water. Although the role of the CNF chemistry was not considered, it was proposed that the active sites for CO_2 adsorption were associated with low-coordination $O^{2-}Mg^{2+}$ sites positioned at the edges and corners on the $Mg(Al)O_x$ nanoparticles, and that there was a higher concentration of these sites on the supported adsorbents. On the other hand, the improved adsorption capacity of the LDH, when supported, must be balanced against the cost and bulk of the support itself. It is useful to consider whether there is an optimum combination that improves the capacity of the sorbent system as a whole, in other words, when normalised to the mass of sorbent plus support.

Multi-walled carbon nanotubes (MWNTs) are attractive materials as a support and can be expected to offer distinct advantages over CNFs, such as 'herringbone' stacks, in which the graphitic sheets lie at an oblique angle terminating at the surface.[16] MWNTs, in principle, have more defined morphology, typically with a smaller diameter, and hence a higher accessible surface area to act as a support. They are very widely available commercially, in large quantities, from a number of companies. Although these bulk materials tend to be relatively defective compared to an ideal MWNT structure, the graphitic layers still lie predominately parallel to the tube axis, giving much greater robustness than CNFs which readily fracture laterally along the oblique basal planes. As a result, MWNT aspect ratios tend to remain high during processing, handling, and subsequent usage, maintaining an effective open framework. Whilst defects in MWNTs lower the chemical and thermal stability, the intrinsic graphitic structure is relatively inert; for CNFs, the basal plane edge terminations provide sites for oxidation, chemical functionalisation, and degradation. Typical, commercially-available CVD-grown MWNTs were used in the present study for simplicity, and ease of replication. Mg–Al LDHs were supported on these MWNTs, using medium to high hydrotalcite loadings, consistent with industrial application, combined with a study of their CO_2 adsorption characteristics.

As synthesised CNTs are generally impure and have a very low solubility/dispersion in common solvents, particularly in water. Therefore, they are often chemically modified to aid their purification and to increase their solubility. A common strategy uses acids or other oxidizing reagents to remove impurities such as metal catalytic particles, amorphous carbon, and graphitic nanoparticles. However, it is now known that these treatments produce molecular oxidation debris (known as 'carboxylated carbonaceous fragments') that can remain adsorbed on the nanotube walls even after conventional water washing. The use of an additional dilute base wash significantly improves purity[17] and may be particularly important in the current context to minimise any CO_2 signal arising from MWNT/debris decomposition. However, the initial oxidation step introduces new oxygen-containing acidic groups that improve water solubility and compatibility with LDH deposition. The final basic treatment converts acidic groups into their conjugate salts, further increasing the solubility of both nanotubes and their oxidation debris, in water; the oxidation debris is washed away, leaving carboxylate sites on the MWNTs. A similar treatment was followed in the present work to provide sites to coordinate metal ions, and balance charge during LDH synthesis. This treatment can be expected to facilitate homogeneous aqueous dispersions of MWNTs for the deposition of LDH crystals by co-precipitation of Mg^{2+} and Al^{3+} ions, under alkaline conditions. In order to study the effect of the MWNT content on the structure and performance of a LDH/MWNT hybrid, a range of samples with different proportions of LDH were prepared and fully characterized. The influence of the MWNTs on the CO_2 sorption capacity of the synthesised hybrids under dry conditions and their performance after continuous adsorption-desorption cycling is reported.

Experimental

Materials

Long, CVD-grown, multi-walled carbon nanotubes (MWNTs) were purchased from ARKEMA (Graphistrength®), with an average diameter of 10–15 nm. $Mg(NO_3)_2 \cdot 6H_2O$ (99%) and $Al(NO_3)_3 \cdot 9H_2O$ (98%) were purchased from Sigma-Aldrich; NaOH, H_2SO_4 (95%), HNO_3 (65%) were purchased from AnalaR and Na_2CO_3 was purchased from Riedel-de Haen. Polycarbonate membranes were from Millipore (HTTP Isopore membrane).

Synthesis of Mg–Al LDHs

Unsupported layered double hydroxides (LDHs) were prepared *via* co-precipitation. An Mg/Al ratio of 2 was selected as it has been reported to be optimal for CO_2 sorption.[18] An aqueous solution (50 mL) of 0.1 mol $Mg(NO_3)_2 \cdot 6H_2O$ and 0.05 mol $Al(NO_3)_3 \cdot 9H_2O$ was added to an aqueous solution (75 mL) containing 0.35 mol of NaOH and 0.09 mol of Na_2CO_3. The resulting white suspension was heated at 333 K for 12 hours under stirring (300 rpm). The resulting precipitate was filtered using 0.4 μm polycarbonate membranes and washed with 500 mL of water at 333 K. Samples were dried for 12 hours at 393 K, under vacuum.

Oxidation of MWNTs

7 mL of a 3:1 mixture of concentrated H_2SO_4/HNO_3 were added for every 200 mg of MWNTs; the acid/MWNT ratio was maintained, since the stoichiometry of the reaction has been shown to be important, although different MWNT masses were used in each experiment. The mixture was stirred and refluxed for 30 min. After cooling, the nanotubes were recovered from the supernatant by filtration using 0.4 μm polycarbonate membranes and washed with 500 mL of 0.01 M NaOH. The solution was then washed with distilled water until the filtrate reached a neutral pH.

Preparation of nanostructured LDH/MWNT hybrids

Oxidised MWNTs were dispersed in an aqueous solution (2.06 mL) containing 9.9 mmol NaOH and 2.5 mmol Na_2CO_3. Subsequently, 1.4 mL of a salt solution of 2.8 mmol $Mg(NO_3)_2 \cdot 6H_2O$ and 1.4 mmol $Al(NO_3)_3 \cdot 9H_2O$ were added. The resulting black suspension was aged at 333 K for 12 hours under stirring (300 rpm). The sample was filtered and dried as

explained above for the preparation of unsupported LDHs. Four different LDH/MWNT hybrids were prepared containing varying LDH weight percentages of 33%, 62%, 73% and 82% using, respectively, 620 mg, 310 mg, 155 mg, and 77.5 mg of oxidised MWNTs at constant LDH precursor concentration.

Calcination of nanostructured LDH/MWNT hybrids

All the materials were calcined prior to CO_2 adsorption measurements at 673 K for 4 hours by flowing 100 mL min^{-1} of N_2 using a tubular quartz reactor (ID = 5 cm) placed in a horizontal Carbolite furnace. Thermal decomposition plays a crucial role in the CO_2 adsorption properties of LDHs. Reddy *et al.*[19] and Hutson *et al.*[20] found that a calcination temperature of 673 K produced LDH derivatives with an optimum balance between surface area and basic sites, which maximized their CO_2 adsorption capacities and favoured reversible adsorption.

Measurements and characterization

X-ray diffraction (XRD) tests were conducted using a PAnalytical X'Pert Pro Multi Purpose Diffractometer (Cu Kα radiation) in reflection mode at room temperature with 2θ varying between 5° and 80°.

Thermogravimetric analysis (TGA) was performed using a Perkin Elmer Pyris 1. 5 mg samples were first dried at 373 K under N_2 for 20 minutes and then heated from 373 to 1073 K at 10 K min^{-1} in 20 mL min^{-1} of air. Transmission electron microscopy (TEM) images were obtained on a JEOL 2010, operating at 200 kV. Samples were prepared by dispersing the sample in isopropanol using 0.01 mg of LDH/MWNT per mL of solvent, and allowing a drop to dry onto a holey carbon copper grid (300 mesh, Agar Scientific). Scanning electron microscopy (SEM) images were collected using Gemini 1525 FEGSEM, fitted with an Oxford Instruments INCA energy dispersive X-ray spectrometer (EDS). SEM images represent bulk dried powder whereas, for TEM, LDH/MWNT material was first dispersed in isopropanol. Nitrogen adsorption and desorption isotherms were measured at 77 K using a Micromeritics Tristar 3000 apparatus on 100 mg pre-dried LDH/MWNT samples held overnight under N_2 prior to adsorption measurements. Specific surface areas were calculated according to the Brunauer, Emmett and Teller (BET) equation from the adsorption isotherm. The pore-size distribution of LDH/MWNT samples was calculated from desorption branch using the Barrett, Joyner, and Halenda method.

Temperature programmed desorption (TPD) of CO_2 was carried out using a quartz micro-flow-column system operated at atmospheric pressure. The sample (20 mg) was preconditioned by heating from room temperature to 673 K at 10 K min^{-1} by flowing 45 mL min^{-1} of Ar. After cooling to 313 K, the sample was exposed to a 20% CO_2/Ar premixed gas (BOC) for 1 hour. The system was then purged in flowing Ar for 2 hours to remove physisorbed CO_2, and the temperature was then increased to 1023 K at 50 K min^{-1}. A mass spectrometer (ESS GeneSys II with capillary sample line) was used to monitor the CO_2 concentration in the quartz tube exit gas stream. Prior to each TPD experiment the response was calibrated by injecting 2 mL of the premixed CO_2 gas.

CO_2 adsorption measurements

A thermogravimetric analyser (TA Instruments, TAQ500) was used to determine the adsorption capacity of pre-calcined samples. An amount (~5 mg) of adsorbent was activated *in situ* to remove CO_2 captured from the atmosphere during its storage and transportation. In a typical measurement, the sample was heated from room temperature to 673 K at 10 K min^{-1} by flowing 60 mL min^{-1} of N_2 and held for 1 hour. The temperature was then decreased to the required adsorption temperature (typically 573 K), and the feed was switched to a 20% CO_2/N_2 premixed gas (BOC), and held usually for 2 hours. The adsorption capacity of the materials was determined from the change in mass during the adsorption step. Effects due to changes in gas viscosity and gas density were taken into account by measuring the response of silicon carbide and then subtracting it from the adsorbent response. Under the operating conditions used, this blank response was very small. The regeneration and stability of the adsorbents were assessed by multicycle tests, in which the adsorption step was carried out at 573 K for 1 hour by flowing the premixed CO_2 gas and the desorption step was performed at 673 K for 30 minutes by flowing nitrogen. The flow rate was kept constant at 60 mL min^{-1} during the experiment.

Results and discussion

LDH/MWNT hybrids were synthesised with differing relative compositions. The TEM (Fig. 1) identified small, crystalline, hexagonal platelets, typical of LDH, attached to the MWNTs. These platelets were about 30 nm and 10 nm in the lateral and through-thickness directions, respectively; the typical nanotube diameter was around 10 nm. No isolated LDH platelets were found in the TEM images; all appeared associated with CNTs, though often present as clusters of a number of LDH platelets, particularly at higher LDH loadings. *In situ* EDS analysis confirmed the presence of C, O, Mg and Al, with the intended Mg/Al ratio of two. It seems that the interaction between the positively-charged LDH sheets and negatively-charged oxidised MWNTs, successfully led to the deposition of LDHs on the support, during the synthesis. The SEM (Fig. 2) of the dried LDH/MWNT powder shows a porous, agglomerated powder, with a uniform dispersion of MWNTs; as expected, an increase in the number of particles was observed, with increasing weight percentage of LDH introduced onto the MWNTs, although no other morphological differences were apparent.

Three stages of weight loss were observed in the TGA pattern of the LDH/MWNT hybrids (Fig. 3). The first weight loss, at approximately 483 K, is attributed to the removal of loosely-bound water molecules from the LDH interlayer. The second weight loss, in the temperature range 483–733 K, is due to the removal of OH^- groups and carbonate anions present in the interlayer space. The third and final weight loss, observed in the temperature range of 733–1073 K, is primarily due to the oxidation of MWNT although some decarbonation of the remaining carbonate anions can also take place.

The actual LDH weight percentage in the sample can be estimated from the residue. The TGA residue of the unsupported LDH material is composed of ~60 wt% mixed solid oxides. The residue of MWNTs is composed of around 8 wt% metallic

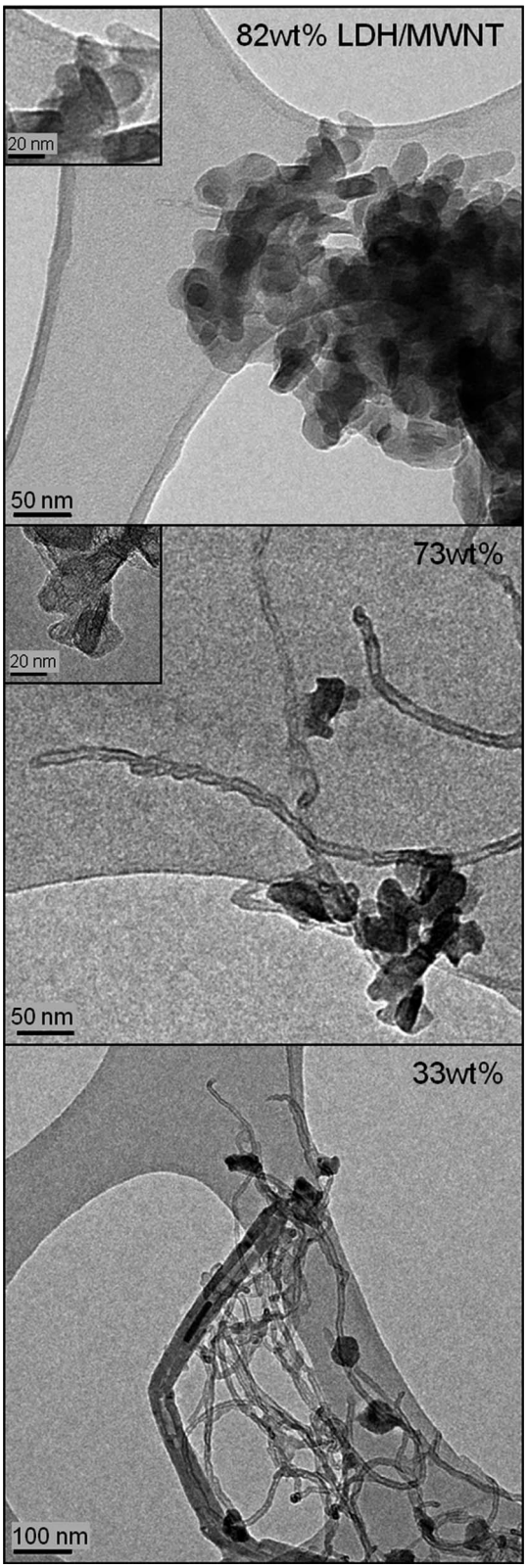

Fig. 1 Representative TEM images corresponding to LDH/MWNT samples.

nanoparticles that were the original catalyst for the nanotube growth, after oxidation during the TGA combustion oxidised during the TGA combustion. Assuming that the residues from each phase are simply additive, the actual LDH weight percentage supported on the nanotubes can be calculated (Fig. 3). The measured MWNT content is systematically slightly lower than expected as the absolute loading is reduced, which is probably due to losses during filtering whilst a filter cake becomes established. Previous syntheses of LDH/MWNT hybrids did not report the actual sample composition.[21,22]

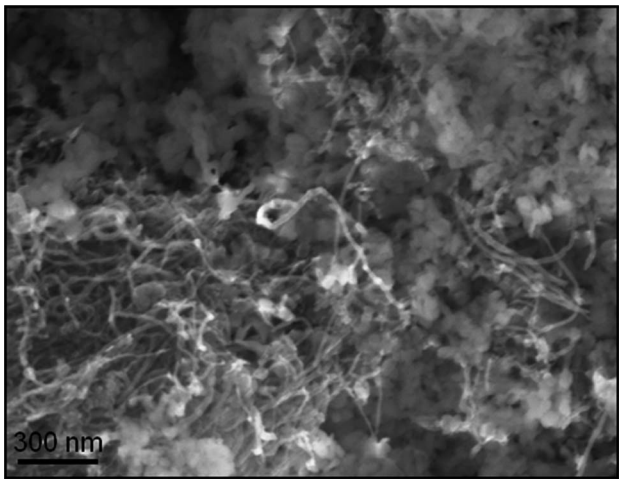

Fig. 2 Representative SEM image of supported 73 wt% LDH/MWNT.

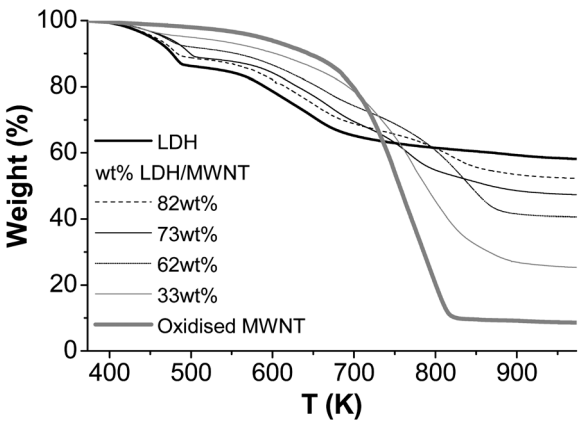

Fig. 3 Thermograms of unsupported LDH, oxidised MWNT and LDH/MWNT hybrid samples.

By combining the TGA with the EDS data (Mg/Al ratio of two), the molecular formula of the dehydrated sample can be expressed as follows: $Mg_{0.66}Al_{0.33}(OH)_2(CO_3)_{0.15}\cdot nH_2O$; where the water content estimated from the TGA corresponds to n = 0.5 mol.

The XRD patterns of all the LDH-containing samples (Fig. 4b–f) display the characteristic reflections corresponding to two-dimensional hydrotalcite-like materials (JCPDS No. 14-191) and can be indexed accordingly.[23] The reflection peak at 26.3° in the XRD patterns of LDH/MWNT samples is indexed to the (002) plane of graphitic carbon (JCPDS No. 41-1487), visible in the pure oxidised MWNT XRD pattern (Fig. 4a). No other crystalline phases were detected. For the hybrid samples, the intensities of the LDH reflections decrease relative to the MWNT (002) peak, as expected on increasing the MWNT loading.

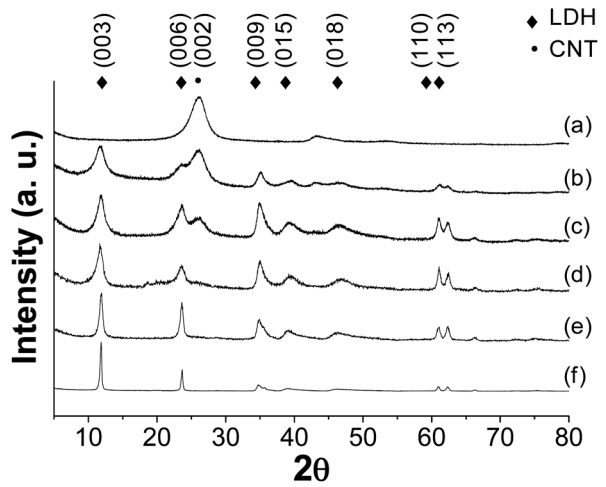

Fig. 4 XRD diffraction patterns of (a) oxidised MWNT, (b) 33 wt% LDH/MWNT, (c) 62 wt%, (d) 73 wt%, (e) 82 wt%, and (f) unsupported LDH. The wt% are estimated by TGA.

The XRD, therefore, confirms that the hybrids contain the intended pure phases. However, the (003) LDH peak broadens (see Fig. 5) with increasing MWNT concentration, either due to a reduction in crystallite size, or an increasing defect concentration. The apparent size or coherence length in the *c*-direction (layer-stacking direction), as calculated by the Scherrer equation, decreases from 15 nm in the 82 wt% LDH/MWNT to 5 nm in the 33 wt% LDH/MWNT. Suggestions[21] that single-walled carbon nanotubes (SWNTs), with an average diameter of 2 nm, can intercalate in LDH seem unlikely to be relevant to the much larger MWNTs used in this work. In addition, the peak positions are unchanged, ruling out variations in interlayer LDH spacing due to hydroxyl-mediated interactions between LDH and MWNTs.[21,22] TEM analyses do not indicate any significant change in LDH platelet thickness; most are around 10 nm thick in all LDH/MWNT sample compositions (a representative TEM image is included in the ESI†). Peak broadening can result from structural disorder, specifically the appearance of stacking faults.[24] The presence of MWNTs during the LDH growth may introduce defects into the LDH structure, through modified nucleation conditions, or induced curvature. One possible defect type is the hypothesis proposed previously by Meis *et al.*[15] who attributed an increase in CO_2 adsorption capacity to a greater number of LDH edge sites when supported. The reproducibility of the LDH/MWNT synthesis was confirmed by repetition of all four LDH/MWNT hybrids; variations in XRD and TGA characterisation were negligible.

The ionic interaction between the negatively-charged oxidised MWNTs and positively-charged LDH nanosheets is expected to play an important role in the LDH growth process. The concentration of carboxylic acid groups introduced onto the oxidised MWNT was estimated by reverse titration as described elsewhere.[17,25] From the titration curve shown in Fig. 6, we estimate the carboxylic acid concentration on the acid oxidised MWNT to be 3.4 mmol g^{-1}. Taking into account the surface area of the oxidised MWNT (191 m^2 g^{-1}) we can estimate a surface charge density of 18 (μmol e^-) m^{-2}. In the case of the LDH, the extra positive charge due to the Al^{3+} substitution is equivalent to 0.33 e per mol of LDH, within the area of the octahedral unit = $\sqrt{3}$ (a^2/2) corresponding to 8.067 $Å^2$, as reported elsewhere.[26] Consequently, the excess LDH surface charge density is around 6.7 (μmol e^+) m^{-2}. In the typical LDH structure, this positive charge is balanced by anions (mostly carbonates); however, it is clear that the negative surface charge density on the MWNTs is on the same order of magnitude. Thus, the tendency of the LDH to nucleate on, and remain associated with the MWNT surface, is reasonable. These electrostatic interactions may both modify the nature of the LDH (as shown in the XRD data) and control the stability of the hybrid.

Surface area measurements show type IV isotherms according to the IUPAC classification, representing a mesoporous adsorbent with strong adsorbent-adsorbate interaction (isotherms are included in the ESI†).[27] The pore-size distribution moves to larger values when the LDH concentration increases in the hybrid samples (Fig. 7), although the mesopore volume does not change with the LDH weight percentage. These trends imply much larger pore sizes present in the LDH system in comparison with MWNTs. We attribute the majority of the pore volume to the open space between the particles, although there also may be a small contribution due to internal spaces (either the hollow core of the MWNTs or the interlayer LDH galleries). The micropore volume appears negligible, as reported by others.[15]

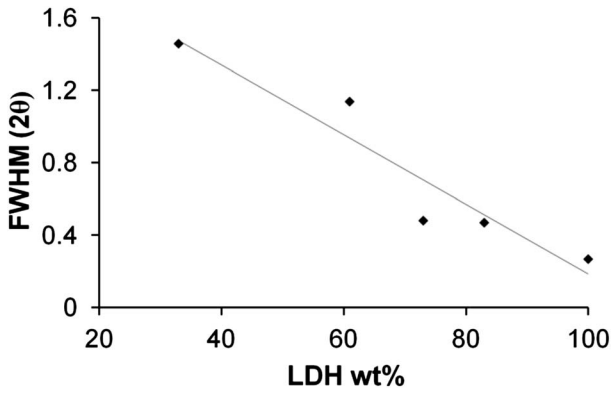

Fig. 5 Full Width at Half Maximum (FWHM) of the (003) peak as a function of LDH weight percentage in the LDH/MWNT hybrids.

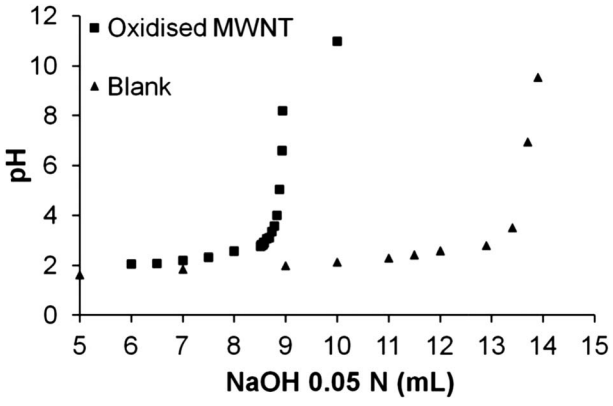

Fig. 6 Titration curves corresponding to the oxidised MWNT and to the blank without nanotubes.

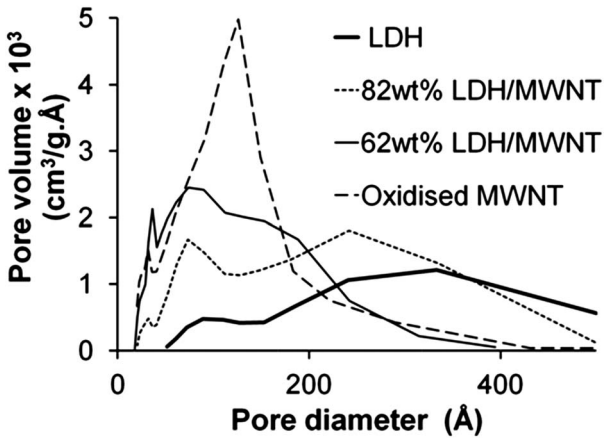

Fig. 7 Pore-size distribution of LDH, oxidised MWNT and LDH/MWNT samples calculated from desorption branch using the Barrett, Joyner, and Halenda method.

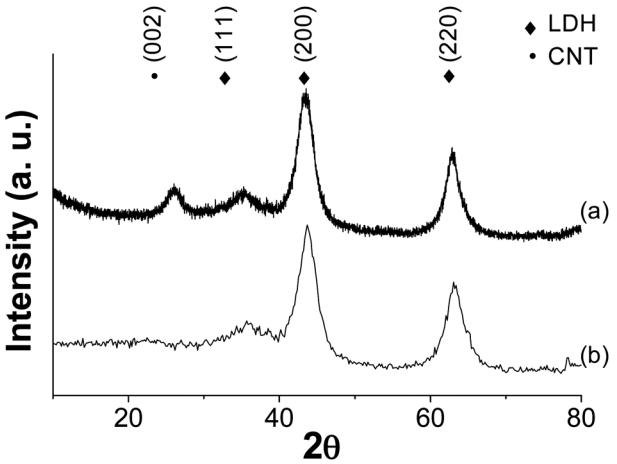

Fig. 9 XRD pattern of (a) calcined 82 wt% LDH/MWNT and (b) calcined unsupported LDH.

By BET adsorption, the surface area of the pure LDH was found to be 64 $m^2 g^{-1}$; the surface area of the hybrids increased consistently with increasing nanotube content, up to the pure MWNTs, at 223 $m^2 g^{-1}$ (Fig. 8). After oxidation, this value drops to 191 $m^2 g^{-1}$, probably due to dense repacking.[28] The potential variation in packing makes it difficult to conclude more firmly whether the surface area follows a simple rule of mixtures, or whether there is a subtle systematic trend due to changes in intrinsic crystal morphology; however, dramatic changes in LDH surface area (such as would accompany a change in crystal thickness from 15 to 5 nm) can be ruled out. Heat treatment of the LDH-containing samples does not significantly alter their specific surface area. However, calcination of the oxidised MWNT increased the surface area significantly, presumably due to the removal of surface oxides and hence improved nitrogen access.

After calcination of the LDH, the resulting mixed metal oxides lose the characteristic XRD patterns (Fig. 9) associated with the layered LDH structure. Only weak, broad peak reflections at 37°, 43°, and 62° were observed, which correspond to diffraction by the (111), (200) and (220) planes of periclase (MgO, JCPDS No. 45-946); the aluminium is thought to be well-dispersed.[29] It is worth noting that recent neutron data shows the structure of the periclase maps rather closely to the original LDH, with much less rearrangement than seems to be implied by the XRD data.[30]

Temperature programmed desorption (TPD) of CO_2 showed that there are a range of strongly-bonded carbonates in the saturated activated (calcined) LDH that are desorbed during the analysis (Fig. 10). The CO_2 uptake of the pure calcined LDH sample, obtained by subtracting the corresponding blank, was 0.44 mol CO_2 kg^{-1} LDH; the desorption was distributed over three overlapping peaks with maxima at 423 K, 543 K and 813 K. The high temperature state can be deconvoluted into two states centred at 813 K and 963 K. These basic sites of increasing strength have been assigned previously to the release of bicarbonates formed on Brønsted OH^- groups (low temperature), bidentante carbonates bonded to metal-oxygen pairs (intermediate temperature) and monodentate carbonates adsorbed on low-coordination oxygen anions (high temperature).[2,31] The low and intermediate energy states are the main contributors to the total adsorption capacity of the activated LDH (Fig. 10). Feasible applications of activated LDHs can be found at temperatures near 423 K for low temperature applications (*e.g.* CO_2 recovery from flue gases) and near 543 K for processes

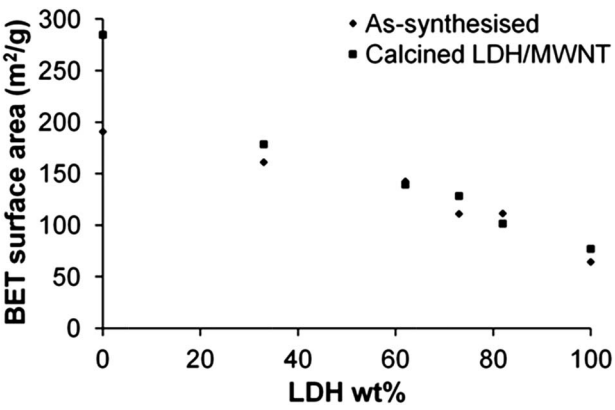

Fig. 8 The BET surface area as a function of LDH weight percentage for the as-synthesised and calcined LDH/MWNT samples.

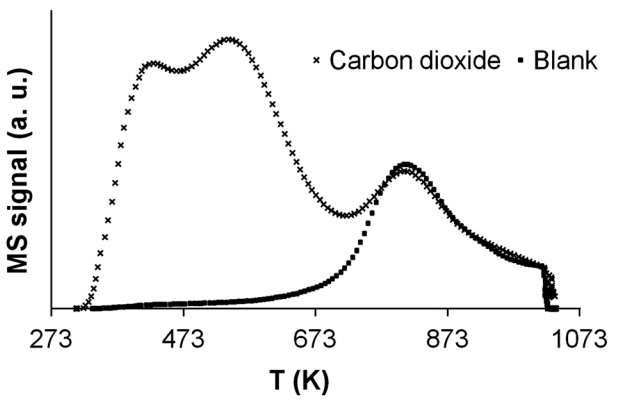

Fig. 10 CO_2-TPD of the activated LDH following pretreatment at 673 K and adsorption at 313 K. The blank was subjected to pretreatment only.

requiring higher operating temperatures (*e.g.* sorption enhanced hydrogen production). In the former case, full advantage of the basicity is taken, whereas the latter case benefits from a low regeneration temperature gradient (543–673 K), which is desirable for temperature swing processes. This study focuses on intermediate temperature applications so that adsorption and desorption temperatures of 573 K and 673 K respectively were considered as representatives to assess the performance of the supported adsorbents. Under these conditions, it is mainly the desorption state centred at 543 K that is cyclically populated and depopulated.

At 573 K, both the unsupported and supported adsorbents exhibited fast initial kinetics achieving more than 80% of their equilibrium capacity within 30 minutes, followed by a slow increase in adsorption capacity (Fig. 11). For practical purposes, the adsorption capacities of the materials were taken at 120 minutes after CO_2 exposure. As observed in Fig. 11, under the operating conditions used, the contribution from the MWNTs is small compared to the LDH CO_2 uptake in all cases, even after considering the normalisation to LDH content discussed below. It is important to consider this control since the MWNTs may themselves weakly adsorb CO_2; the competition between this adsorption and decomposition of remaining surface oxides (carboxylate groups), or slow etching of amorphous carbon/defect sites by CO_2, is probably responsible for the gentle maximum observed. Any etching is expected to be very modest at the temperatures applied,[32] as evidenced by the cycling stability discussed below. For intrinsically less stable supports, such as CNFs, or in the presence of water, these background effects may be more significant.

The CO_2 adsorption capacity of the materials was taken as the average of at least 5 measurements under the same operating conditions. The adsorption capacity of the pure LDH showed good reproducibility among the set of tests performed (standard deviation of 0.02). On the other hand, the carbon supported samples exhibited variable adsorption capacities with standard deviations between 0.06 and 0.15. This result was attributed to heterogeneity in the material on the scale of mass used for TGA (5 mg). However, there is a clear trend showing that the mean adsorption capacity per mass of LDH under dry conditions increases as the LDH content is reduced (Fig. 12). Meis *et al.*[15] reported enhanced adsorption capacities of LDHs supported on carbon nanofibers but no clear relation between the CO_2 capacity and textural properties of the materials was found, in contrast to the present study. The adsorption capacities given in Fig. 12 are comparable to results obtained from LDH supported on zeolites[14] when differences in adsorption temperature and loading are taken into account. However, they are lower than those reported for the CNF system[15] (1.3–2.5 mol CO_2 kg LDH^{-1}). These previous values are not directly comparable with the present work since the CO_2 adsorption was carried out in the presence of water, which is known to increase greatly the adsorption capacity of LDHs.[5,6,33] The results were also obtained at a lower adsorption temperature (which increases adsorption) and at lower LDH loadings which, as can be seen from Fig. 12, tends to increase specific adsorption capacity.

The enhancement in adsorption capacity observed in this study can be related to a changed characteristic of the LDH since the MWNTs surface itself only contributes very weakly. One possibility is increased accessibility due to the improved particle dispersion of supported LDH, or other increase in effective LDH surface area due to changes in crystal thickness or quality. The possible appearance of stacking faults due to the presence of MWNTs during LDH growth, may also contribute positively to the adsorption capacity, by creating more active sites. Lastly, the dispersion of the LDH on the MWNT support is likely to mitigate sintering during calcination leading to a more active and stable material.

The regeneration and stability of the adsorbents were assessed by carrying out continuous adsorption-desorption cycles under dry conditions (see Fig. 13). The unsupported LDH exhibited a steep initial fall followed by a slow decline in adsorption capacity. The trend observed is consistent with that of other studies (also performed under dry conditions), which have attributed the first stage to a small amount of CO_2 irreversibly chemisorbed in the LDH.[5,6,10] Although the carbon-supported samples also showed this behaviour, the stability of the pure LDH was clearly increased by the dispersion on the MWNTs (Figs. 13 and 14). Ding *et al.*[6] found that the initial loss in adsorption capacity observed in LDHs under dry conditions is mitigated by the presence of water possibly by maintaining the hydroxyl concentration of the surface and/or preventing site

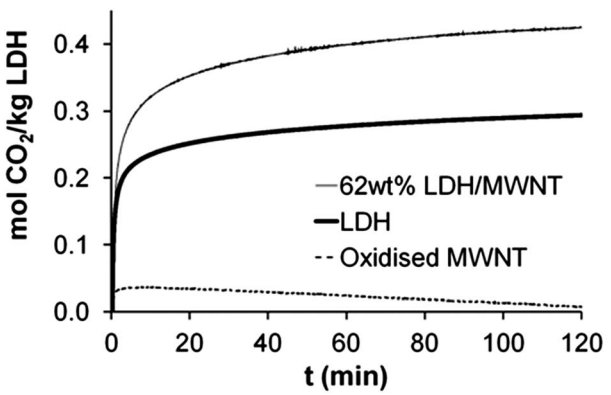

Fig. 11 Representative CO_2 adsorption profiles of the LDH, 62 wt% LDH/MWNT and oxidised MWNT, at 573 K and $P(CO_2) = 0.2$ bar. Oxidised MWNT curve referred to mol CO_2 kg^{-1} of product.

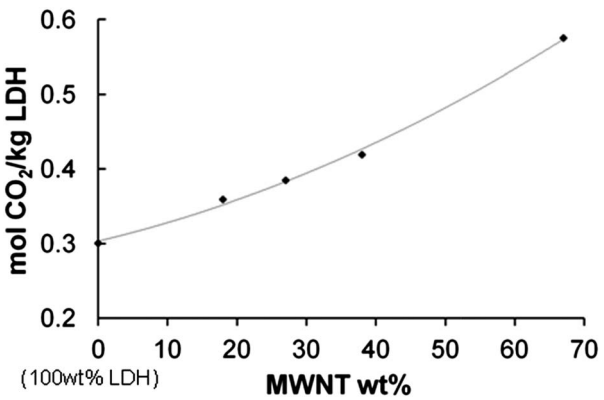

Fig. 12 Average CO_2 sorption capacities per mass of LDH of the pure hydrotalcite and carbon hybrids as a function of the MWNT content in the material at 573 K and $P(CO_2) = 0.2$ bar.

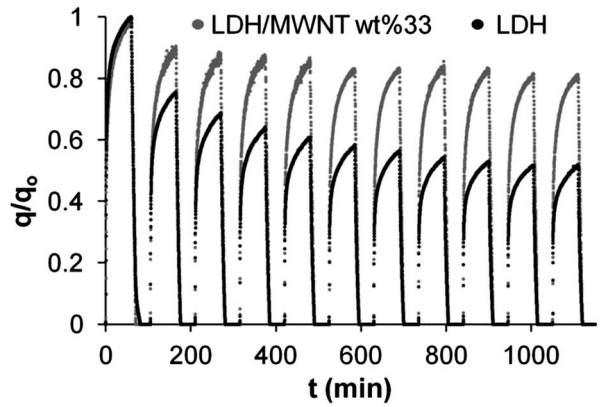

Fig. 13 Multicycle profile of the activated LDH (black) and 33 wt% LDH/MWNT (grey) at 573 K.

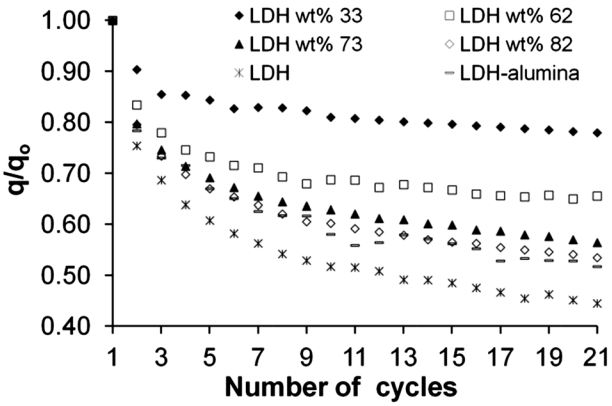

Fig. 14 Normalised CO_2 adsorption capacity over 21 adsorption-desorption cycles.

poisoning through carbonate or coke deposition. Similarly, under hydrated adsorption conditions, CO_2 capacity was reported to be constant for both pure and CNF-supported LDHs over 10 cycles,[15] masking any specific stabilising effect of the support.

It is known that alumina adds thermal stability to LDH.[13] Therefore, the performance of the carbon hybrids was compared with that of a commercial adsorbent consisting of 20:80 LDH:α-alumina by weight. The stability of the alumina-based adsorbent was superior to that of the unsupported LDH. However, it was evident that the carbon-supported LDHs were markedly more stable than the alumina adsorbent even at high total LDH content (Fig. 14). The improvement may be attributed to the strong network forming ability of MWNTs in contrast to the relatively low surface area of α-alumina.

Although a clear enhancement in adsorption capacity per mass of LDH is achieved by supporting LDH on MWNTs (Fig. 12), it is also important to consider the adsorption capacity per mass of total adsorbent (*i.e.* LDH + MWNTs) since this parameter has a greater impact for industrial application. The adsorption capacity per mass of adsorbent was found to increase with the LDH loading in the sample during the first adsorption-desorption cycle. However, as the number of cycles increases the trend in adsorption capacity is reversed since the supported adsorbents

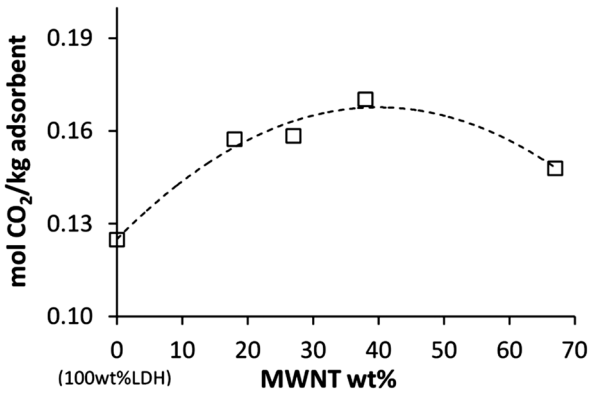

Fig. 15 Average CO_2 sorption capacities per mass of total adsorbent corresponding to the 21st cycle of the pure hydrotalcite and carbon hybrids as a function of the MWNT content in the material at 573 K and $P(CO_2) = 0.2$ bar.

are significantly more stable. After 21 cycles the adsorption capacity of the pure LDH is 20 to 40% lower (depending on the LDH loading) than that of the LDH/MWNTs hybrids. Fig. 15 shows clearly that, when normalizing to total mass of adsorbent, there is an optimum LDH loading corresponding to 35–50 wt% MWNTs.

Conclusions

We report an *in situ* layered double hydroxide (LDH) precipitation onto base-washed, oxidised, multi-walled carbon nanotubes (MWNTs) as a facile strategy to fabricate hybrid materials, due to a compatible degree of surface charge. The CO_2 adsorption capacity per mass of hydrotalcite of the activated LDH materials was shown to increase when supported on MWNTs. Increases in the effective surface area and in the structural disorder of the supported materials are the two factors that may contribute to enhance the adsorbent/gas contact and therefore, the specific adsorption capacity. The stability of the LDH materials was increased significantly when supported on MWNTs. Consequently, after adsorption-desorption cycling under dry conditions, there is an optimum LDH loading (about 60 wt% LDH) in terms of adsorption capacity per total mass of adsorbent. Previous work has shown that water plays an important role in mitigating loss of adsorption capacity in supported LDHs and improving performance; on the other hand, the stability of carbonaceous supports in the presence of water, particularly during higher temperature desorption steps must also be considered. Whilst the fundamental performance of the LDH/MWNT is best explored initially under dry conditions, further studies should consider the impact of water on the adsorption performance in order to understand potential industrial application as a sorbent system in a variety of contexts. Other uses of optimised MWNT/LDH hybrids may also emerge, for example as electrochemical electrodes or polymer fillers.[34,35]

Acknowledgements

The authors are grateful to Felicity Sartain, Almudena Celaya-Sanfiz, Maurice C. D. Mourad, Neal Skipper, Stephen Hodge, Robert Menzel and Jose Luis Pinilla Ibarz for discussions and

help during experiments. Financial support for this project was provided by the Deanship of Scientific Research at King Abdulaziz University T/81/429 and scholarships from CONACYT and SEP.

Notes and references

1 L. Feng and X. Duan, in *Layered Double Hydroxides*, eds. X. Duan and D. G. Evans, Springer-Verlag Berlin, Berlin, 2006, pp. 193–223.
2 D. P. Debecker, E. M. Gaigneaux and G. Busca, *Chem.–Eur. J.*, 2009, **15**, 3920–3935.
3 S. Choi, J. H. Drese and C. W. Jones, *ChemSusChem*, 2009, **2**, 796–854.
4 Q. A. Wang, J. Z. Luo, Z. Y. Zhong and A. Borgna, *Energy Environ. Sci.*, 2011, **4**, 42–55.
5 J. R. Hufton, S. Mayorga and S. Sircar, *AIChE J.*, 1999, **45**, 248–256.
6 Y. Ding and E. Alpay, *Chem. Eng. Sci.*, 2000, **55**, 3461–3474.
7 Y. Ding and E. Alpay, *Chem. Eng. Sci.*, 2000, **55**, 3929–3940.
8 E. R. van Selow, P. D. Cobden, P. A. Verbraeken, J. R. Hufton and R. W. van den Brink, *Ind. Eng. Chem. Res.*, 2009, **48**, 4184–4193.
9 B. T. Carvill, S. Nataraj, J. R. Hufton, S. G. Mayorga, T. R. Gaffney, J. R. Brzozowski, *Pat.*, 00101685.6, 2000.
10 N. D. Hutson and B. C. Attwood, *Adsorpt.-J. Int. Adsorpt. Soc.*, 2008, **14**, 781–789.
11 H. T. J. Reijers, S. E. A. Valster-Schiermeier, P. D. Cobden and R. W. van den Brink, *Ind. Eng. Chem. Res.*, 2006, **45**, 2522–2530.
12 E. L. G. Oliveira, C. A. Grande and A. E. Rodrigues, *Sep. Purif. Technol.*, 2008, **62**, 137–147.
13 O. Aschenbrenner, P. McGuire, S. Alsamaq, J. W. Wang, S. Supasitmongkol, B. Al-Duri, P. Styring and J. Wood, *Chem. Eng. Res. Des.*, 2011, **89**, 1711–1721.
14 M. R. Othman, N. M. Rasid and W. J. N. Fernando, *Chem. Eng. Sci.*, 2006, **61**, 1555–1560.
15 N. Meis, J. H. Bitter and K. P. de Jong, *Ind. Eng. Chem. Res.*, 2010, **49**, 8086–8093.
16 M. L. Toebes, J. M. P. van Heeswijk, J. H. Bitter, A. Jos van Dillen and K. P. de Jong, *Carbon*, 2004, **42**, 307–315.
17 R. Verdejo, S. Lamoriniere, B. Cottam, A. Bismarck and M. Shaffer, *Chem. Commun.*, 2007, 513–515.
18 J. I. Yang and J. N. Kim, *Korean J. Chem. Eng.*, 2006, **23**, 77–80.
19 M. K. R. Reddy, Z. P. Xu, G. Q. Lu and J. C. D. da Costa, *Ind. Eng. Chem. Res.*, 2006, **45**, 7504–7509.
20 N. D. Hutson, S. A. Speakman and E. A. Payzant, *Chem. Mater.*, 2004, **16**, 4135–4143.
21 H. Wang, X. Xiang and F. Li, *J. Mater. Chem.*, 2010, **20**, 3944–3952.
22 S. Huang, H. D. Peng, W. W. Tjiu, Z. Yang, H. Zhu, T. Tang and T. X. Liu, *J. Phys. Chem. B*, 2010, **114**, 16766–16772.
23 F. Millange, R. I. Walton and D. O'Hare, *J. Mater. Chem.*, 2000, **10**, 1713–1720.
24 D. Tichit, M. N. Bennani, F. Figueras and J. R. Ruiz, *Langmuir*, 1998, **14**, 2086–2091.
25 H. Hu, P. Bhowmik, B. Zhao, M. A. Hamon, M. E. Itkis and R. C. Haddon, *Chem. Phys. Lett.*, 2001, **345**, 25–28.
26 H. T. Zhao and K. L. Nagy, *J. Colloid Interface Sci.*, 2004, **274**, 613–624.
27 K. S. W. Sing, D. H. Everett, R. A. W. Haul, L. Moscou, R. A. Pierotti, J. Rouquerol and T. Siemieniewska, *Pure Appl. Chem.*, 1985, **57**, 603–619.
28 M. S. P. Shaffer, X. Fan and A. H. Windle, *Carbon*, 1998, **36**, 1603–1612.
29 M. Leon, E. Diaz, S. Bennici, A. Vega, S. Ordonez and A. Auroux, *Ind. Eng. Chem. Res.*, 2010, **49**, 3663–3671.
30 M. C. D. Mourad, M. Mokhtar, M. G. Tucker, E. R. Barney, R. I. Smith, A. O. Alyoubi, S. N. Basahel, M. S. P. Shaffer and N. T. Skipper, *J. Mater. Chem.*, 2011, **21**, 15479–15485.
31 J. I. Di Cosimo, C. R. Apesteguia, M. J. L. Gines and E. Iglesia, *J. Catal.*, 2000, **190**, 261–275.
32 S. Delpeux, K. Szostak, E. Frackowiak and F. Béguin, *Chem. Phys. Lett.*, 2005, **404**, 374–378.
33 M. K. R. Reddy, Z. P. Xu, G. Q. Lu and J. C. D. da Costa, *Ind. Eng. Chem. Res.*, 2008, **47**, 2630–2635.
34 V. Georgakilas, D. Gournis, M. A. Karakassides, A. Bakandritsos and D. Petridis, *Carbon*, 2004, **42**, 865–870.
35 B. X. Du and Z. P. Fang, *Nanotechnology*, 2010, **21**, 315603.

